Available at www.sciencedirect.com

ScienceDirect

journal homepage: www.elsevier.com/locate/he

Analysis of entropy generation in hydrogen-enriched methane–air propagating triple flames

Alejandro M. Briones[a,*], *Achintya Mukhopadhyay*[b], *Suresh K. Aggarwal*[c]

[a]*University of Dayton Research Institute, Energy and Environmental Engineering Division, Modeling and Simulation Group, 300 College Park, Dayton, OH 45469, USA*

[b]*Mechanical Engineering Department, Jadavpur University, Kolkata 700032, India*

[c]*Mechanical and Industrial Engineering, University of Illinois at Chicago, Chicago, IL 60607, USA*

ARTICLE INFO

Article history:
Received 2 July 2008
Received in revised form
18 September 2008
Accepted 18 September 2008
Available online 30 November 2008

Keywords:
Entropy generation
Hydrogen-enriched methane flame
Second law analysis
Propagating triple flame

ABSTRACT

A theoretical–numerical analysis based on the second law of thermodynamics is used to examine the propagation of laminar H_2-enriched CH_4–air flames. The analysis is based on computing the various entropy generation terms in a transient reacting flow field. A comprehensive, time-dependent computational model, which employs a detailed description of chemistry and transport, is used to simulate the transient ignition and flame propagation in this reacting flow field. Flames are ignited in a jet-mixing layer far downstream of the burner. Following ignition, a well-defined triple flame is formed that propagates upstream with nearly constant flame displacement speed along the stoichiometric mixture fraction line. As the flame approaches the burner, it transitions to a double flame, and subsequently to a burner-stabilized nonpremixed flame. The triple point exhibits the maximum entropy generation, indicating that this point is characterized by high chemical reactivity, as well as large temperature and mass fraction gradients. The volumetric entropy generation is the highest in the two premixed reaction zones, and the lowest in the nonpremixed reaction zone. In the premixed zones, the volumetric entropy generation due to chemical reaction is the highest, followed by heat conduction, and then mixing. The converse is true for the nonpremixed zone. However, the integrated entropy generation rate indicates that heat conduction is the major contributor, followed by chemical reactivity, and then mixing. As H_2 addition to methane fuel is increased, the integrated entropy generation increases primarily due to enhanced heat conduction and chemical reactivity. However, the contributions of heat conduction, chemical reactivity, and mixing to total entropy generation weakly depend on the fuel being burned. While the flame propagates upstream entropy generation increases and reaches a maximum when the flame exhibits a well-defined triple flame structure, and then decreases as the flame approaches the burner. The second law efficiency of the system remains nearly constant with H_2 addition, since the increased irreversibilities due to H_2 addition are compensated by the increase in the flow availability in the fuel blend.

* *Corresponding author*. Tel.: +1 937 255 2162; fax: +1 937 252 9917.
E-mail address: alejandro.briones.ctr@wpafb.af.mil (A.M. Briones).

0360-3199/$ – see front matter © 2008 International Association for Hydrogen Energy. Published by Elsevier Ltd. All rights reserved.
doi:10.1016/j.ijhydene.2008.09.103

Nomenclature

A_{in}	availability at inlet, W
$\overline{a}_{a,in}$	availability of air at the inlet, J/kg
$\overline{a}_{f,in}$	availability of fuel at the inlet, J/kg
$D_{i\text{-}mix}$	mass diffusivity of species i in mixture, m^2/s
$\overline{e}_i$	specific molar internal energy, J/mol
e^{ch}	chemical availability, W
f_i	body force per unit volume of species i, N/m^3
$\overline{g}_{f,i}$	Gibbs free energy of formation of species "i" at reference pressure and temperature, J/kmol
$\mathbf{j}_i$	mass flux of species i, kg/m^2s
p_i	partial pressure of species i, Pa
P	total pressure, Pa
P_{ref}	reference total pressure, Pa
$\mathbf{q}_c$	conduction heat flux, W/m^2
r	radial coordinate, m
R	gas constant, J/kg K
$\overline{R}$	universal gas constant, J/kmol K
S	specific entropy, J/kg K
s_i	specific entropy of species i, J/kg K
$\overline{s}_i^0$	specific entropy of species i at reference pressure, J/kg K
T	temperature, K
T_0	temperature of environment, K
v_r	radial velocity, m/s
v_z	axial velocity, m/s
x_i	mole fraction of species i, dimensionless
y_i	mass fraction of species i, dimensionless
z	axial coordinate, m

Greek symbols

υ_i	stoichiometric mole coefficient of species
μ	viscosity, Pa s
μ_i	chemical potential of species i, J/kg K
ρ	density, kg/m^3
σ	integrated entropy generation rate, W/kg K
σ'''	volumetric entropy generation rate, W/m^3 K
τ	viscous stress, N/m^2
ω_I	production rate of species i, kg/m^3 s

Subscripts

cond	conduction
mix	mixing
tot	total
vis	viscous effect

1. Introduction

Analysis based on second law of thermodynamics has been utilized to optimize design and improve performance of energy systems [1–4]. Combustion of fuel involves complex interaction of different physical and chemical processes. Since many of these processes are irreversible and involve loss of exergy, they have important implications in devices like gas turbines and internal combustion engines. Thus, in order to improve the performance of different combustion systems, it is essential to identify the causes of irreversibility.

The majority of analysis on entropy generation in systems involving heat and mass transfer are based on the formulation of Hirschfelder et al. [5]. While there has been numerous works on entropy generations in nonreacting flows involving heat and mass transfer [6,7], there has been relatively less work dealing with entropy generation in combustion systems. A comprehensive account of exergy analysis in combustion systems is available in a recent review by Som and Datta [8].

Puri [9], Dash and Som [10] and Hiwase et al. [11] analysed the entropy generation associated with combustion of an isolated droplet. While Puri [9] based his analysis of entropy generation mainly on empirical values of transport coefficient, Dash and Som [10] and Hiwase et al. [11] solved the detailed conservation equations to obtain the flow and scalar fields. Both Dash and Som and Hiwase et al. observed that for a stationary droplet where the combustion is diffusion-controlled, the major contributor to the entropy generation is the heat conduction.

Arpaci and Selamet [12] used dimensional analysis to study entropy generation in premixed flames on a flat flame burner. They found that the minimum quenching distance for the flame corresponds to an extremum in entropy generation. Nishida et al. [13] analysed entropy generation and exergy loss in both premixed and diffusion flames. For premixed flames, they considered laminar, steady one-dimensional flow, and observed that chemical reaction is the dominant contributor to entropy generation, although its contribution changes with flame structure modification and temperature. Li et al. [14] considered entropy generation in the flame zone of a cylindrical microcombustor. They used one-dimensional analysis and an approximate relation for temperature distribution in the flame zone, and concluded that entropy generation reaches a minimum at the quenching radius and that stoichiometric mixtures give most irreversible combustion.

Dunbar and Lior [15] calculated irreversibilities in hydrogen and methane premixed and nonpremixed flames. They separated the entropy generation into three processes: combined diffusion and fuel oxidation, internal thermal energy exchange and product constituent mixing. Their analysis identified internal energy exchange as the major constituent of entropy generation. Datta [16] investigated entropy generation in confined axisymmetric laminar diffusion flames and observed that the largest share of entropy generation comes from transport processes. The analysis further showed that air preheating reduced entropy generation while heat loss through the confining wall increased the irreversibility. In their analysis of nonpremixed flames, Nishida et al. [13] also concluded that for axisymmetric laminar diffusion flames heat conduction accounts for the largest fraction of entropy generation. Datta [17] investigated the effect of gravity on entropy generation in axisymmetric laminar diffusion flames. The study concluded again that at all gravity levels, heat transfer remains the major source of irreversibility.

All the above works consider only steady premixed or nonpremixed flames. However, many engineering applications like internal combustion engines involve propagating

flames. Often these flames are partially premixed (triple flame) in nature while in transit. In local quenching of non-premixed flames [18] and propagation and stabilization of flames in axisymmetric jets [19], flames develop into partially premixed mode of combustion, containing double and triple flame structures [20–23]. In the realm of turbulent flames, local extinction and re-ignition give rise to partially premixed flames. The process of re-ignition can involve the formation of a triple flame that may lose its characteristics during propagation [24]. Under certain conditions a propagating triple flame may lose one or both of its premixed wings and degrade into a double or diffusion flame [25,26]. This transition is of both fundamental and practical interest. In direct injection spark ignition engines (DISI), fuel is injected directly into the combustion chamber just prior to ignition, resulting in an inhomogeneous mixture distribution in the combustion chamber at the time of injection. The flame front propagates through locally rich and locally lean pockets of fuel–air mixture burning in a partially premixed mode [27].

The propagating flames in all these configurations generally have a partially premixed character, i.e., they contain both premixed and nonpremixed branches. Hence, the results of earlier investigations, dealing with only premixed or only nonpremixed flames are not directly applicable for such devices. The objective of this investigation is to study entropy generation in a propagating triple flame, and its subsequent transition to a double flame and then to a nonpremixed flame structure. The study is based on a complete analysis involving the detailed simulations of propagating triple flames. The synergy between the premixed and the nonpremixed branches is expected to have significant effect on the dominant entropy generation processes. Hence, the results are post-processed to obtain the individual contributions of viscous dissipation, heat conduction, mixing, and chemical reactivity processes to total entropy generation. All the previous studies on entropy generation in gaseous flames consider only pure fuels. However, it is of interest to characterize entropy generation in flames burning fuel blends. Moreover, there is significant interest in developing hydrogen-based and hydrogen-enhanced combustion systems. Therefore, it is important for practical applications to understand how hydrogen addition affects the irreversibilities as well as exergy in hydrocarbon-air flames. Considering these, the effect of hydrogen addition on entropy generation in propagating methane–air flames is also investigated.

2. Mathematical modeling

The mathematical model is presented in two parts. The first part deals with the simulation of propagating flames in non-premixed or partially premixed jets, based on the solution of the time-dependent conservation equations for an axisymmetric unsteady reacting flow. This has been described in detail elsewhere [28–30] and hence is only briefly discussed here. The second part deals with the computation of irreversibilities or entropy generation in propagating triple flames, and is described in more detail in this paper.

The time-dependent conservation equations for two-dimensional (axisymmetric) unsteady reacting flows have been discussed in our previous studies [28,29]. An optically thin gas model is used in the energy equation to account for thermal radiation from the flame. The thermodynamic and transport properties appearing in the governing equations are temperature and species dependent, the details of which are given elsewhere [19,28,29]. The methane–air chemistry is modeled using the GRI-Mech. 1.2, which considers 31 species and 346 elementary reactions [31]. The major species included in the mechanism are CH_4, O_2, CO_2, CO, CH_2O, H_2, H_2O, C_2H_2, C_2H_4, C_2H_6, CH_3OH, and N_2, while the radical species include CH_3, CH_2, CH, CHO, H, O, OH, HO_2, H_2O_2, C_2H, C_2H_3, C_2H_5, CHCO, C, $CH_2(s)$, CH_2OH, CH_3O, CH_2CO, and HCCOH. The numerical algorithm employs a time-accurate finite-volume approach using a staggered, non-uniform grid system. The algorithm as well as the reaction mechanism has been validated previously for the computation of premixed flame speeds and the detailed structure of premixed, partially premixed and nonpremixed flames [32–34].

3. The entropy transport equation

The flow field and the distribution of scalar properties, such as temperature and species mass fractions, are obtained from numerical solutions of the governing equations. From the flow and scalar field distributions, the local entropy generation rate is computed using the entropy transport equation, which is obtained in the following form [35]:

$$\rho\frac{s}{t}=\left[-\nabla\cdot\left(\frac{\mathbf{q}_c}{T}\right)-\sum_i\nabla\cdot(\mathbf{j}_i s_i)\right]+\left[\frac{\tau:\nabla V}{T}-\frac{\mathbf{q}_c\cdot\nabla T}{T^2}-\frac{1}{T}\sum_i \mathbf{j}_i\cdot(s_i\nabla T+\nabla\mu_i)+\sum_i\frac{\mathbf{f}_i\cdot\mathbf{j}_i}{T}-\sum_i\frac{\mu_i\omega_i}{T}\right] \quad (1)$$

The terms within the first bracket of right hand side represent the rate of entropy transport, while those within the second bracket represents the entropy generation due to different effects, and are the focus of the present study. These include entropy generation due to viscous dissipation, heat conduction, mixing (or mass diffusion), body forces, and chemical reaction, respectively. Assuming Fourier law and Fick's Law, one can write $\mathbf{q}_c=-k\nabla T$ and $\mathbf{j}_i=-\rho D_{i-mix}\nabla y_i$. Also using $\nabla\mu_i+s_i\nabla T=\nabla\mu_i^T=(RT/x_i)\nabla x_i$ for ideal gases, the expression for entropy generation becomes

$$\sigtt_{total}=\frac{\tau:\nabla V}{T}+\frac{k\nabla T\cdot\nabla T}{T^2}+R\sum_i\frac{\rho D_{i-mix}}{x_i}\nabla y_i\cdot\nabla x_i+\sum_i\frac{\mathbf{f}_i\cdot\mathbf{j}_i}{T}-\sum_i\frac{\mu_i\omega_i}{T} \quad (2)$$

For cases where gravity is the only body force, $\sum\mathbf{f}_i\cdot\mathbf{j}_i=\sum\mathbf{g}\cdot\mathbf{j}_i=\mathbf{g}\cdot\sum_i\mathbf{j}_i=0$. Thus, the expression for entropy generation becomes

$$\sigtt_{total}=\frac{\tau:\nabla V}{T}+\frac{k\nabla T\cdot\nabla T}{T^2}+R\sum_i\frac{\rho D_{i-mix}}{x_i}\nabla y_i\cdot\nabla x_i-\sum_i\frac{\mu_i\omega_i}{T} \quad (3)$$

Assuming Newtonian fluids and an axisymmetric flame configuration, the final form of volumetric entropy generation rate can be written as

$$\sigtt_{total}=\sigtt_{vis}+\sigtt_{cond}+\sigtt_{mix}+\sigtt_{chem} \quad (4)$$

The contributions of the individual processes to the entropy generation are expressed as

$$\sigma'''_{vis} = \frac{\mu}{T}\left[2\left\{\left(\frac{\partial v_r}{\partial r}\right)^2+\left(\frac{v_r}{r}\right)^2+\left(\frac{\partial v_z}{\partial z}\right)^2\right\} + \left(\frac{\partial v_r}{\partial z}+\frac{\partial v_z}{\partial r}\right)^2 - \frac{2}{3}\left(\frac{1}{r}\frac{\partial (r\cdot v_r)}{\partial r}+\frac{\partial v_z}{\partial z}\right)^2\right]$$

$$\sigma'''_{cond} = \frac{k}{T^2}\left[\left(\frac{\partial T}{\partial r}\right)^2+\left(\frac{\partial T}{\partial z}\right)^2\right]$$

$$\sigma'''_{mix} = R\rho\sum_i \frac{D_{i-mix}}{x_i}\left[\frac{\partial y_i}{\partial r}\frac{\partial x_i}{\partial r}+\frac{\partial y_i}{\partial z}\frac{\partial x_i}{\partial z}\right]$$

$$\sigma'''_{chem} = -\sum_i \frac{\mu_i \omega_i}{T}$$

For an ideal gas mixture:

$$\mu_i = \bar{e}_i(T) - T\cdot \bar{s}^0_i(T) + \bar{R}T\ln\left(\frac{x_i P}{P_{ref}}\right)$$

where $P_{ref} = 1$ atm and $\bar{s}^0_i(T)$ is the reference entropy of species "i" at P_{ref}. The upper bar indicates a property per unit mole. The units of chemical potential (μ_i) and species reaction rate (ω_i) are in J/mol and mol/m^3 s, respectively. The units of entropy generation σ'''_{total} are J/(m^3 s K). Eq. (4) can now be used to obtain the entropy generation due to viscous dissipation, thermal conduction, mixing, and chemical reaction for propagating flames in an axisymmetric configuration. The integrated entropy generation rate can be obtained using the equation:

$$\sigma = \int\int 2\pi r \sigma''' \, dr\, dz \tag{5}$$

Then the second law efficiency (η_{II}) is obtained using the following equation [36]:

$$\eta_{II} = 1 - \frac{T_0\sigma}{A_{in}} \tag{6}$$

Here T_0 *is the dead temperature which is taken as the ambient temperature (i.e.* $T_0 = 300$ *K). The availability at the inlet is calculated as follows [8,36].*

The inflow availability is given as [36]

$$A_{in} = h - h_0 - T_0(s - s_0) + \frac{V^2}{2} + gz + e^{ch} \tag{7}$$

Here, h is the enthalpy, s the entropy, V the velocity, g the gravitational acceleration, z the height, R the universal gas constant, and e^{ch} the chemical exergy. The subscript "0" refers to the dead state conditions. In our simulations the dead state corresponds to the ambient conditions (i.e. 300 K and 1 atm). All terms on the right hand side except the last one represent the thermomechanical exergy (availability) flow. The potential and kinetic exergy can be considered negligible. Since our inlet conditions are considered as ambient conditions (i.e. dead state), $h = h_0$, and $s = s_0$, all terms are 0 expect the last one, and the above equation can be written as

$$A_{in} = e^{ch} = \dot{m}_{a,in}a_{a,in} + \dot{m}_{f,in}a_{f,in} \tag{8}$$

The units of A_{in}, $\dot{m}$, and a are kW, kg/s, and kJ/kg, respectively. For air and fuel entering as separate streams at the reference temperature ($T_{f,in} = T_{a,in} = T_{ref}$) and reference total pressure ($p_{a,in} = p_{ref}$ and $p_{f,in} = p_{ref}$), the above equations simplify to [36]

$$\bar{a}_{a,in} = 0 \tag{9}$$

$$\bar{a}_{f,in} = \bar{g}_{f,f} + \nu_{O_2}\bar{g}_{f,O_2} - \nu_{CO_2}\bar{g}_{f,CO_2} - \nu_{H_2O}\bar{g}_{f,H_2O(g)} + \bar{R}T_{ref}\ln\frac{x^e_{O_2}{}^{\nu_{O_2}}}{x^e_{CO_2}{}^{\nu_{CO_2}}\, x^e_{H_2O(g)}{}^{\nu_{H_2O}}} \tag{10}$$

Here $\bar{g}_{f,i}$ the molar Gibbs free energy of species i, and υ_i the stoichiometric mole coefficient of species i. x^e_i the mole fraction of ith species in the environment, which is composed of 21% O_2, and 79% N_2. Using the composition of the environment as given by Szargut et al. [37], Moran and Shapiro [36] computed the exergy of methane and hydrogen in the gaseous state as 831,650 and 236,100 kJ/kmol, respectively, based on the above equation. Note that these values are lower than their respective HHV, which are 888,160 and 283,560 kJ/kmol for methane and hydrogen, respectively. Using the composition given in this text, and calculating the exergy directly, we obtain the following values for the various methane–hydrogen blends: $\bar{a}_{f,in} = 792,998$ kJ/kmol for 100:0 (CH_4:H_2) blend; $\bar{a}_{f,in} = 651,389$ kJ/kmol for 75:25 blend, $\bar{a}_{f,in} = 509,781$ kJ/kmol for 50:50 blend; and $\bar{a}_{f,in} = 368,172$ kJ/Kmol for 25:75 blend. The slight differences between our values and those obtained by Moran and Shapiro [36] are due to different environment compositions used. In addition, note that the values of $\bar{a}_{f,in}$ are close to their respective LHV. For instance, LHVs for the mixtures given above are 802,405, 662,265, 522,125, and 381,985 kJ/kmol, respectively. In fact, the ratios of $\bar{a}_{f,in}$/LHV for the mixtures given above is 1.012, 1.017, 1.024, and 1.038, respectively.

The specific flow exergy is calculated from molar exergy as

$$a_{f,in} = \frac{\bar{a}_{f,in}}{M_f} \tag{11}$$

The corresponding $a_{f,in}$ for the above four methane-hydrogen above are 50,150, 52,981, 58,013, and 69,431 kJ/kg, respectively.

4. Solution procedure

The finite-difference forms of the momentum equations are obtained using QUICKEST scheme [38], while those of the species and energy are obtained using a hybrid scheme of upwind and central differencing. The pressure field is calculated at every time step by solving all of the pressure Poisson equations simultaneously.

Fig. 1 illustrates the computational domain. It consists of 100 mm × 50 mm in the axial (z) and radial (r) directions, respectively, and is represented by a staggered, non-uniform grid system (601 × 201). We have examined the grid resolution issues previously [39], and found that a minimum grid spacing of 0.05 mm is sufficient to resolve the flame structure, including H and CH radical layers. Consequently, the minimum grid spacing is 0.05 mm in both the r- and z-directions, and the reported results are nearly grid independent. An isothermal insert (2 × 0.8 mm) is used to simulate the inner burner wall. The temperature at the burner wall was set at 300 K. The inner and outer jets are assumed to have uniform velocity profiles, with velocities of 10 cm/s and 30 cm/s, respectively. The inner jet issues a H_2–CH_4 mixture, while the outer jet issues air. A propagating flame is established by

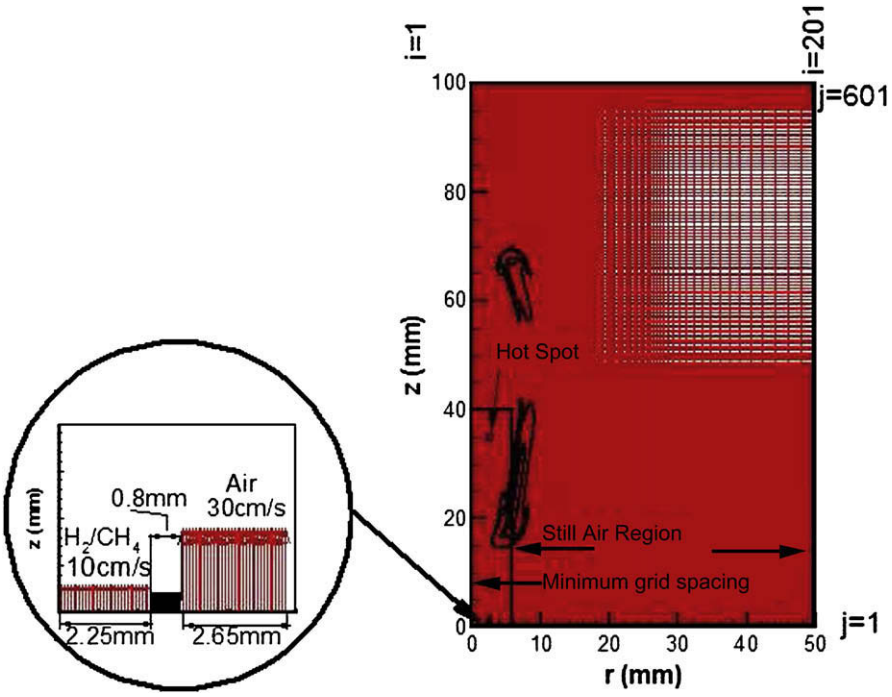

Fig. 1 – Schematic of the computational domain and grid used in the simulations. The small rectangle shows the minimum grid spacing region where the propagating flame front is located.

simulating ignition in the far field (35 mm above the burner rim) of the jet-mixing layer. The ignition event is simulated by providing a high-temperature zone of 2000 K in a small rectangular cross-sectional area (2 mm^2), containing small amounts of H and OH radicals. This generates an ignition kernel that propagates upstream and rapidly develops into a triple flame, which then propagates upstream towards the burner rim and eventually stabilizes at the rim.

5. Results and discussion

Fig. 2 presents the simulated results of transient ignition, flame propagation and its subsequent stabilization for a propagating CH_4-air flame in a nonpremixed jet. The snapshots or instantaneous images are depicted in terms of heat release rate contours. The image at $t = 0$ ms corresponds to the instant when the high-temperature ignition source is removed, while the subsequent images show the formation and propagation of a triple flame. Following ignition, two reacting volumes are formed, as indicated by the image at $t = 3$ ms. One volume propagates downstream and is quickly extinguished. The other propagates upstream towards the burner and develops into a propagating triple flame, which is the focus of this investigation. The triple flame structure develops at $t \sim 18$ ms. The flame then propagates in a quasi-steady manner, i.e., at near-constant flame displacement speed, from $z = 25$ mm to $z = 4$ mm, exhibiting a well-defined triple flame structure as indicated in the snapshot at 48 ms. The three reaction zones, namely the rich premixed zone (RPZ), the lean premixed zone (LPZ), and the nonpremixed zone (NPZ), can be readily identified in the 18 ms and 48 ms images. As the flame approaches the burner rim (i.e. $z \approx 4$ mm), the length of the RPZ shortens, and the flame transitions to a double flame, i.e., the LPZ extinguishes. The flame reaches the burner rim at 88 ms, and during its stabilization at the rim, the RPZ extinguishes and the flame transitions from a double flame to a steady nonpremixed flame.

Fig. 3 presents the volumetric entropy generation rate (cf. Eq. (4)) contours for two propagating triple flames in 100%CH_4–0%H_2 and 50%CH_4–50%H_2 nonpremixed jets, respectively. For both the flames, the maximum volumetric entropy generation rate occurs at the triple point, which is shared by the three reaction zones. Although the individual entropy generation contributions peak at the triple point, the entropy generation rate due to chemical reaction is about 2.8 times larger than that due to heat conduction, which in turn is significantly higher than that due to mixing. This indicates that the triple point is characterized by high chemical reactivity as well as large temperature and mass fraction gradients. Then, the entropy generation rate due to chemical reactions decreases slowly along the two premixed reaction zones, but rather rapidly along the nonpremixed reaction zone. In the two premixed zones, entropy generation due to chemical reaction is the highest, followed by heat conduction, and then mixing. On the contrary, in the nonpremixed branch, entropy generation due to mixing is the highest, followed by heat conduction, and then chemical reaction. Previous studies [13,16,17] have shown that in nonpremixed flames, entropy generation due to heat conduction is the highest. Therefore, the synergy between the multiple branches alters the dominant chemical and physical processes responsible for entropy generation in the nonpremixed branch of the triple flames with respect to the corresponding nonpremixed flames. Nevertheless, the dominant entropy generation process in the premixed branches remains the same as that observed previously for premixed flames [13].

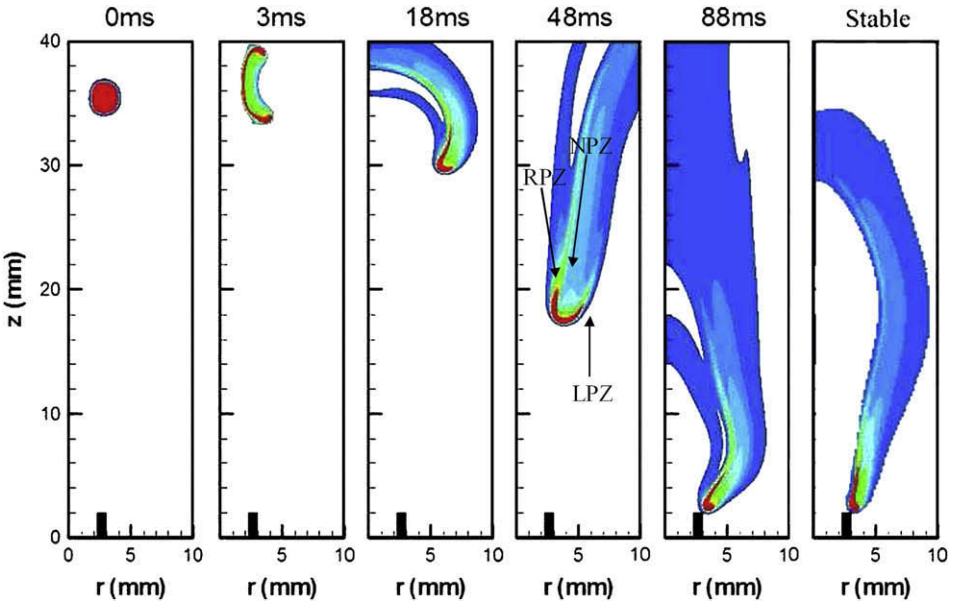

Fig. 2 – Snapshots in terms of heat release rate contours showing the temporal evolution of ignition and flame propagation in the mixing layer of methane and coflowing air jets. The three reaction zones, i.e., the rich premixed (RPZ), nonpremixed (NPZ), and lean premixed (LPZ) zones, are indicated in the snapshot at t = 48 ms.

Moreover, while the dominant entropy generation in both the premixed branches is due to chemical reaction, the contribution from the rich premixed branch is higher than that from the lean premixed branch due to a higher volume of the former. It is also seen that the entropy generation due to heat conduction is significant over a larger region with H_2 addition, implying that H_2 addition increases entropy generation primarily through heat conduction.

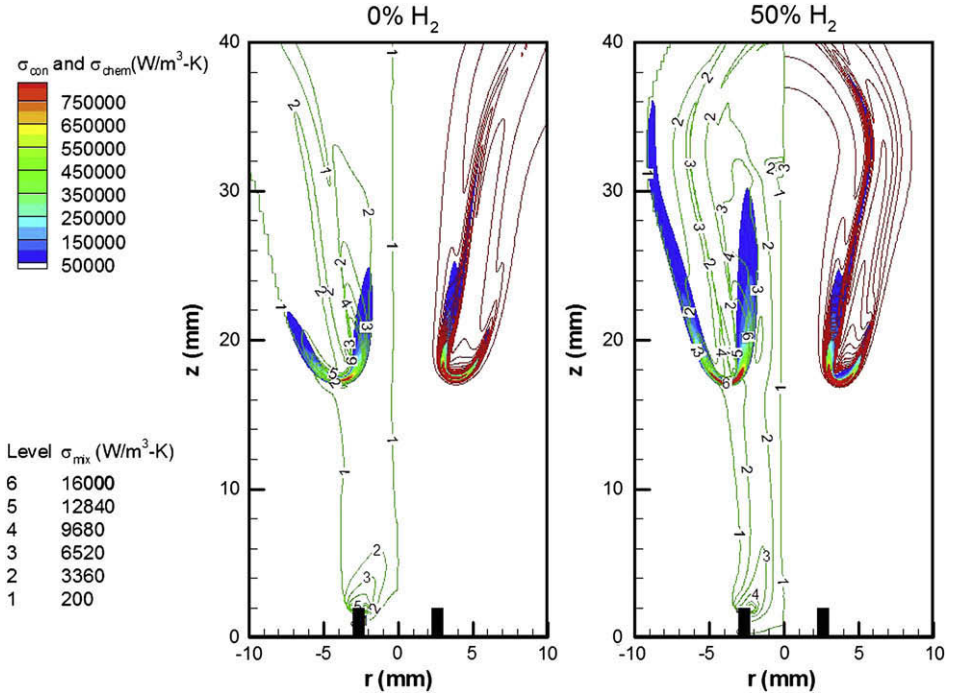

Fig. 3 – Entropy generation and heat release rate contours (red lines on the right) for two propagating triple flames in 100%CH_4–0%H_2 and a 50%CH_4–50%H_2 nonpremixed jets, respectively. The volumetric entropy generation rate contours due to conduction, chemical reaction, and mixing (mass diffusion) are represented by σ_{CON} (flooded contours on the left), σ_{CHEM} (flooded contours on the right), and σ_{MIX} (green lines on the left), respectively. The two flames are compared at different times, but at the same axial location. [For interpretation of color referred in this figure legend, the reader is referred to web version of the article.]

Fig. 4 presents the relative entropy generation rate due to conduction ($\sigma_{CON}/\sigma_{Total}$), chemical reaction ($\sigma_{CHEM}/\sigma_{Total}$), and mixing ($\sigma_{MIX}/\sigma_{Total}$) as a function of time for the (a) 0%H_2–100%CH_4, (b) 50%H_2–50%CH_4, and (c) 75%H_2–25%CH_4 flames.[1] For a given condition, $\sigma_{MIX}/\sigma_{Total}$ remains nearly constant and substantially less than the other two. With H_2 addition, $\sigma_{CHEM}/\sigma_{TOTAL}$ decreases, whereas $\sigma_{CON}/\sigma_{TOTAL}$ increases during flame propagation. However, for pure methane flames, the relative importance of heat conduction first increases, reaches a maximum and then decreases. Note here that Nishida et al. [13] observed that $\sigma_{CHEM}/\sigma_{TOTAL}$ is lower for pure CH_4–air flames than for pure H_2 flames while our results show that relative importance of chemical reaction decreases with increase in H_2 content. This may be attributed to the fact that the Nishida et al. [13] considered planar premixed flames where entropy generation by chemical reaction is always dominant. In propagating triple flames, entropy generation by heat conduction is the most dominant process contributing to exergy losses, as mentioned previously.

Although Fig. 3 provides a good picture of the local distribution of different components of entropy generation, the overall irreversibility of the system is governed by the entropy generation, integrated over the entire volume. Fig. 5 presents the integrated entropy generation rate due to conduction (σ_{CON}), chemical reaction (σ_{CHEM}), and mixing (σ_{MIX}), as well as the total entropy generation rate (σ_{total}), as a function of H_2 mole fraction in the CH_4–H_2 fuel mixture. For the ease of discussion, Fig. 5 also presents the relative contributions of conduction ($\sigma_{CON}/\sigma_{Total}$), chemical reaction ($\sigma_{CHEM}/\sigma_{Total}$), and mixing ($\sigma_{MIX}/\sigma_{Total}$) to the total entropy generation rate as a function of H_2 mole fraction. Although the premixed branch is characterized by the largest volumetric entropy generation due to chemical reaction, it is the entropy generation due to heat conduction that occupies more volume in the flame (cf. Fig. 3). Therefore, the results in Fig. 5 indicate that heat conduction is the major contributor to the integrated entropy generation. Furthermore, H_2 addition increases the entropy generation primarily due to heat conduction. For instance, as the H_2 content is increased from 0% to 75%, the magnitude of entropy generation due to heat conduction, chemical reaction, and mixing increases by 90%, 71%, and 64%, respectively. For a 75%H_2–25%CH_4 fuel mixture, the thermal conductivity and peak flame temperature are about 3.5 and 1.05 times higher than those for pure CH_4. This indicates that the temperature gradients are reduced with H_2 enrichment in order for σ_{COND} corresponding to the 75%H_2–25%CH_4 flame to be only 1.9 times σ_{COND} corresponding to the pure CH_4 flame. Although H_2 addition increases the total entropy generation, the relative contributions of heat conduction, chemical reaction, and mixing to total entropy generation are not substantially modified. For instance, as the amount of H_2 is increased from 0% to 75%, the fraction of entropy generation due to heat conduction increases non-monotonically from 54% to 58%, whereas that due to chemical reactions and mixing decreases non-monotonically as well from 36% to 34% and from 9.5% to 8.5%, respectively (cf. Fig. 5b). These results show that the relative importance of the different factors contributing to

[1] These relative entropy generation rates are integrated over the entire computational domain so they represent global quantities.

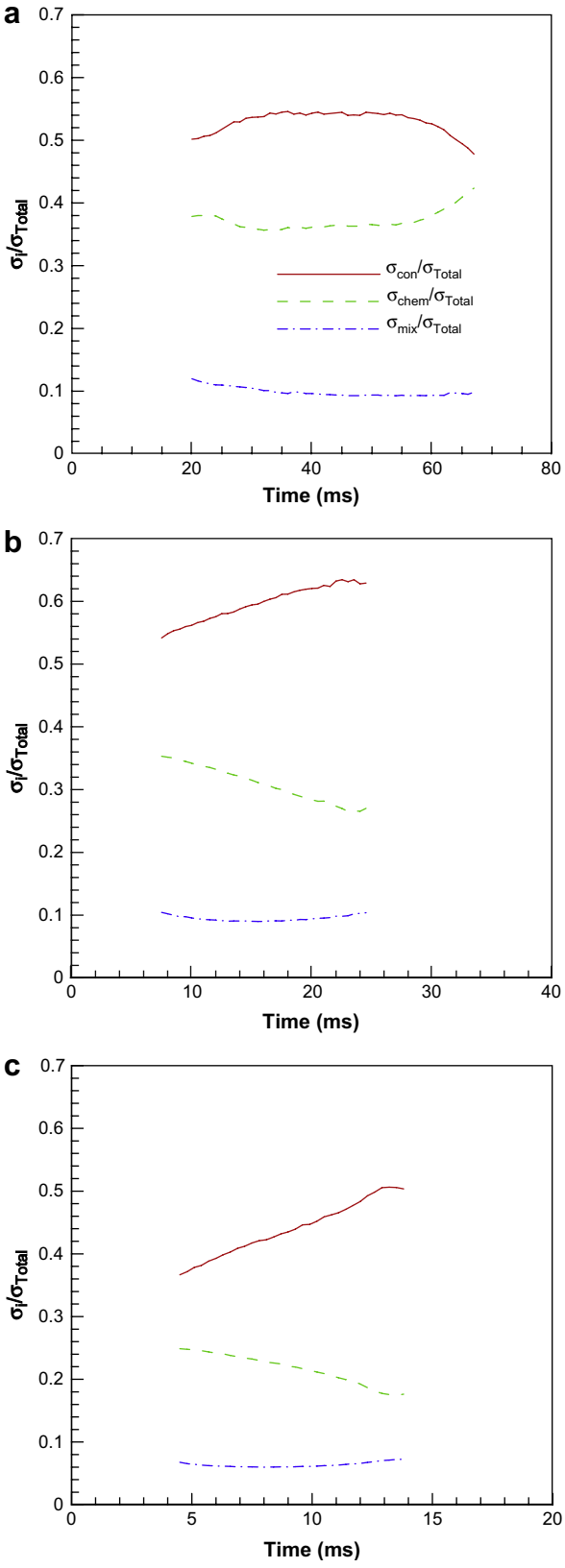

Fig. 4 – Relative entropy generation rate due to conduction ($\sigma_{CON}/\sigma_{Total}$), chemical reaction ($\sigma_{CHEM}/\sigma_{Total}$), and mixing ($\sigma_{MIX}/\sigma_{Total}$) as a function of time for the (a) 0%H_2–100%CH_4, (b) 50%H_2–50%CH_4, and (c) 75%H_2–25%CH_4 flames. Note that σ_i represents the integrated or global values.

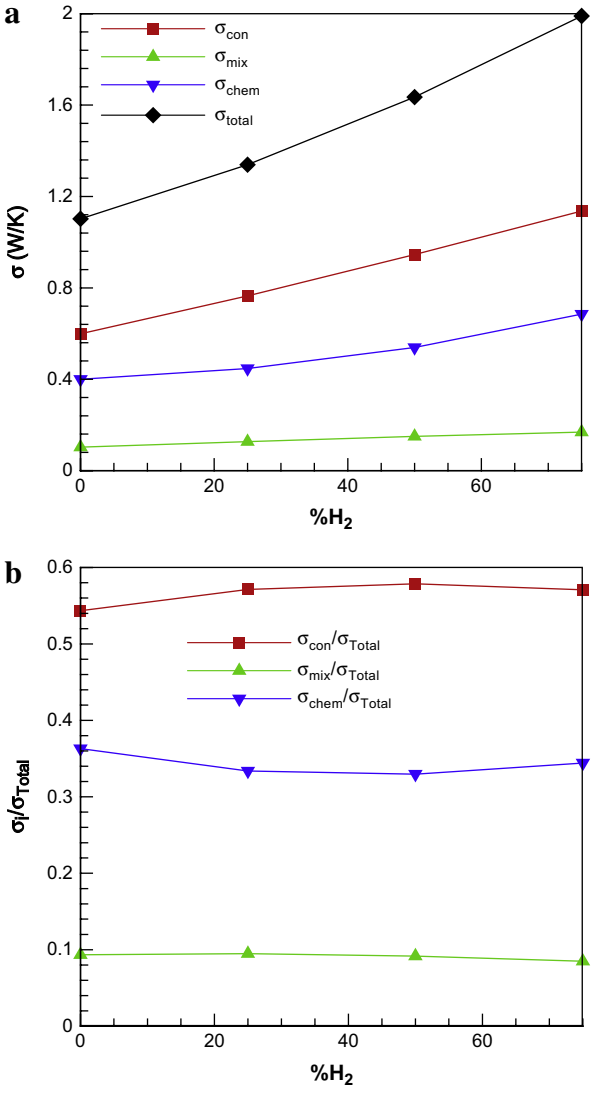

Fig. 5 – (a) Integrated entropy generation rates due to conduction (σ_{CON}), mixing (σ_{MIX}), and chemical reactivity (σ_{CHEM}) as a function of H_2 mole fraction (%). The integrated values are computed at different times, but at the same axial location of the flame, with the triple point located at z = 17 mm. (b) Relative entropy generation rates $\sigma_{CON}/\sigma_{Total}$, $\sigma_{CHEM}/\sigma_{Total}$, and $\sigma_{MIX}/\sigma_{Total}$ as a function of H_2 mole fraction.

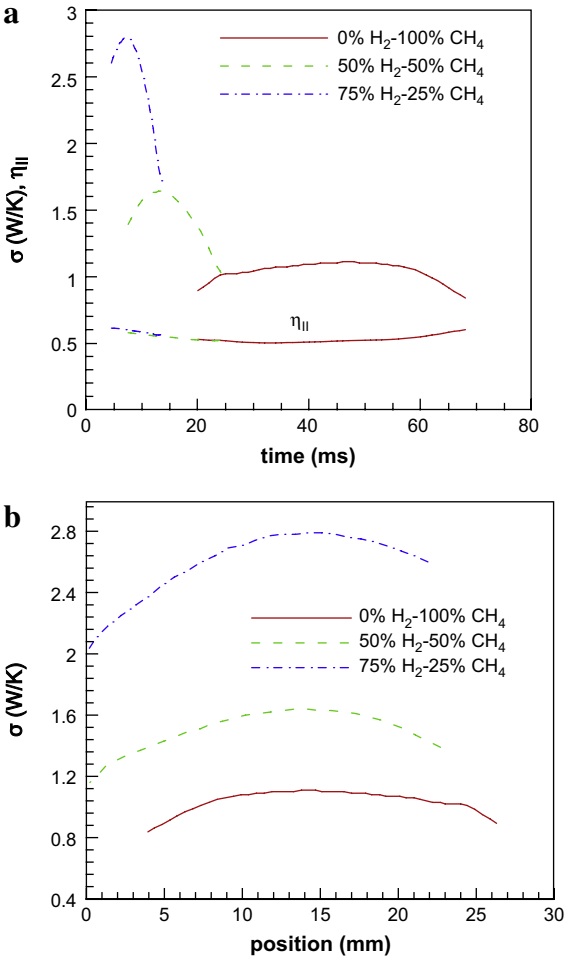

Fig. 6 – (a) Integrated entropy generation rate (σ) and second law efficiency (η_{II}) as a function of time for the 0%H_2–100%CH_4, 50%H_2–50%CH_4, and 75%H_2–25%CH_4 flames; (b) integrated entropy generation rate (σ) as a function of flame position for the same three flames.

entropy generation is not significantly altered by the addition of hydrogen. On the other hand, a comparison with the results of Nishida et al. [13] for plane premixed flames shows the difference in the relative contributions for the two different configurations. Therefore, the relative importance of the major chemical and physical processes that contribute to entropy generation depends on the flame configuration rather than the fuel being burned.

Fig. 6(a) presents the total integrated entropy generation rate (σ) and second law efficiency (η_{II}) as a function of time for the 0%H_2–100%CH_4, 50%H_2–50%CH_4, and 75%H_2–25%CH_4 flames. The entropy generation first increases during flame propagation and reaches a maximum, and then it decreases monotonically until the flame reaches the burner rim and gets stabilized there. Although the total irreversibility of the system increases with addition of hydrogen, the second law efficiency (η_{II}) of the system remains nearly constant with H_2 addition, indicating that the increased irreversibilities (i.e. $T_0\sigma$) due to H_2 addition are compensated by the increased flow availability in the fuel mixture. Notice that the second law efficiency (η_{II}) decreases to a minimum and then it increases with time. The minimum value of the second law efficiency (η_{II}) occurs at the same time when the maximum entropy generation (σ) occurs. Fig. 6(b) presents the integrated entropy generation as a function of flame position. Note that the maximum entropy generation occurs nearly at the same axial position regardless of hydrogen addition. Since the flame structure changes during the transit, this result corroborates our earlier observation that entropy generation in a propagating flame is more dependent on the flame configuration than the fuel composition. A plausible explanation for the initial increase in entropy generation is that chemical reactivity intensifies and the reacting volume increases, as the

ignition kernel develops into a triple flame. Then, as the flame propagates upstream, the mixing layer decreases, weakening the premixed branches. This in turn reduces the chemical reactivity and the temperature and mass fraction gradients; hence the entropy generation decreases.

6. Conclusions

A theoretical–numerical analysis based on the second law of thermodynamics is used to explain the entropy generation in propagating triple flames and the effect of hydrogen enrichment on entropy generation. Propagating triple flames are established in axisymmetric coflowing jets by igniting the fuel–air mixture at a downstream location. A time-accurate implicit algorithm that uses detailed descriptions of transport and fuel chemistry is used for simulations. Then, the total entropy generation, as well as the individual contributions of viscous dissipation, heat conduction, mixing, and chemical reactivity to total entropy generation are post-processed from the simulations. Important conclusions are

1. For all the propagating triple flames investigated, there is no loss of exergy when blending methane with hydrogen. The second law efficiency of the system remains nearly constant with H_2 addition, since the increased irreversibilities due to H_2 addition are compensated by the increase in the flow availability in the fuel blend. This is an important result with the implication that the thermodynamics of the combustion process may not be not significantly altered by the blending of hydrogen.
2. The relative importance of the major chemical and physical processes that contribute to entropy generation depends on the flame configuration rather than the fuel being burned. For instance, regardless of the fuel blend the maximum irreversibilities are observed when the propagating flame exhibits a well-defined triple flame structure.
3. For all four H_2-enriched methane–air flames, the volumetric entropy generation is the highest in the two premixed reaction zones, and the lowest in the nonpremixed reaction zone. In the premixed zones, the volumetric entropy generation due to chemical reaction is the highest, followed by heat conduction, and then by mixing. On the contrary, in the nonpremixed branch, entropy generation due to mixing is the highest, followed by heat conduction, and then by chemical reaction. In typical nonpremixed flames, entropy generation due to heat conduction is the highest. Therefore, the synergy between the multiple branches alters the dominant chemical and physical processes responsible for entropy generation in the nonpremixed branch of the triple flames with respect to their corresponding nonpremixed flames. However, the dominant entropy generation process in the premixed branches remains the same as that observed in premixed flames.
4. The maximum entropy generation occurs at the triple point, indicating that this point is characterized by high chemical reactivity, and large temperature and mass fraction gradients. Thus the triple point can also be identified as the location of highest entropy generation.

REFERENCES

[1] Bejan A. Convection heat transfer. 2nd ed. New York: John Wiley & Sons; 1995.
[2] Shudo Y, Ohkubo T, Hideshima Y, Akiyama T. Exergy analysis of the demonstration plant for coproduction of hydrogen and benzene from biogas. Int J Hydrogen Energy, doi:10.1016/j.ijhydene.2008.06.043.
[3] Toonssen R, Woudstra N, Verkooijen AHM. Exergy analysis of hydrogen production plants based on biomass gasification. Int J Hydrogen Energy 2008;33:4074–82.
[4] Rosen MA, Scott DS. Entropy production and exergy destruction: Part I-hierarchy of Earth's major constituencies. Int J Hydrogen Energy 2003;28:1315–23.
[5] Hirschfelder JC, Curtiss CF, Bird RB. The Molecular Theory of Gases and Liquids. New York: Wiley; 1954.
[6] San JY, Worek WM, Lavan Z. Entropy generation in convective heat transfer and isothermal convective mass transfer. Trans ASME J Heat Transfer 1987;109:647–52.
[7] Carrington CG, Sun ZF. Second law analysis of combined heat and mass transfer phenomena. Int J Heat Mass Transfer 1991;34:2767–93.
[8] Som SK, Datta A. Thermodynamic irreversibilities and exergy balance in combustion processes. Prog Energy Combust Sci 2007;. doi:10.1016/j.pecs.2007.09.001.
[9] Puri IK. Second law analysis of convective droplet burning. Int J Heat Mass Transfer 1992;35:2571–8.
[10] Dash SK, Som SK. Transport processes and associated irreversibilities in droplet combustion in a convective medium. Int J Energy Res 1991;15:603–19.
[11] Hiwase SD, Datta A, Som SK. Entropy balance and exergy analysis of the process of droplet combustion. J Phys D Appl Phys 1998;31:1601–10.
[12] Arpaci VS, Selamet A. Entropy production in flames. Combust Flame 1998;73:251–9.
[13] Nishida K, Takagi T, Kinoshita S. Proc Combust Inst 2002;29: 869–74.
[14] Li ZW, Chou SK, Shu C, Yang WM. Entropy generation during microcombustion. J Appl Phys 2005;97:084914.
[15] Dunbar WR, Lior N. Sources of combustion irreversibility. Combust Sci Tech 1994;103:41–61.
[16] Datta A. Entropy generation in a confined laminar diffusion flame. Combust Sci Tech 2000;159:39–56.
[17] Datta A. Effects of gravity on structure and entropy generation of confined laminar diffusion flames. Int J Thermal Sci 2005;44:429–40.
[18] Favier V, Vervisch L. Edge flames and partially premixed combustion in diffusion flame quenching. Combust Flame 2001;125:788–803.
[19] Qin X, Choi CW, Mukhopadhyay A, Puri IK, Aggarwal SK, Katta VR. Triple flame propagation and stabilization in a laminar axisymmetric jet. Combust Theory Modell 2004;8: 293–314.
[20] Lock A, Briones AM, Aggarwal SK, Puri IK, Hegde U. Combust Flame 2005;143:159–73.
[21] Peters N. Partially premixed diffusion flamelets in non-premixed turbulent combustion. Proc Combust Inst 1984;20: 353–60.
[22] Ruetsch GR, Vervisch L, Liñán A. Effects of heat release on triple flames. Phys Fluids 1995;7(1447).
[23] Flynn PF, Durrett RP, Hunter GL, Loye AO, Akinyemi OC, Dec JE, Westbrook CK. Diesel combustion: An integral view combining laser diagnostics, chemical kinetics, and empirical validation. SAE paper 1999-01-0509; 1999.
[24] Vervisch L. Using numerics to help understanding of nonpremixed turbulent flames. Proc Combust Inst 2000;28: 11–24.

[25] Buckmaster J. Edge flames and their stability. Combust Sci Technol 1996;115:41–68.
[26] Buckmaster J. Edge-flames. Prog Energy Combust Sci 2002;28: 435–75.
[27] Wehrmeyer JA, Cheng Z, Mosbacher DM, Pitz RW. Opposed jet flames of lean or rich premixed propane-air reactants versus hot products. Combust Flame 2002;128:232–41.
[28] Shu Z, Aggarwal SK, Katta VR, Puri IK. Flame-vortex dynamics in an inverse partially premixed combustor: The Froude number effects. Combust Flame 1997;111:276.
[29] Azzoni R, Ratti S, Puri IK, Aggarwal SK. Gravity effects on triple flames: Flame structure and flow instability. Phys Fluids 1999;11:3449.
[30] Qin X, Puri IK, Aggarwal SK, Katta VR. Gravity, radiation and coflow effects on partially premixed flames. Phys. Fluids 2004;16:2963.
[31] Frenklach M, Wang H, Yu C-L, Goldenberg M, Bowman CT, Hanson RK, Gardiner WC, Lissianski V. GRI-Mech – an optimized detailed chemical reaction mechanism for methane combustion. Report no. GRI-95/0058; November 1, 1995. http://www.me.berkeley.edu/gri_mech/.
[32] Egolfopoulos FN, Zhu DL, Law CK. Experimental determination of laminar flame speeds: mixtures of C2-hydrocarbons with oxygen and nitrogen. Proc Combust Inst 1990;23:471.
[33] Heard DE, Jeffries JB, Smith GP, Crosley DR. LIF measurements in methane/air flames of radicals important in prompt NO formation. Combust Flame 1992;88:137.
[34] Katta VR, Takahashi F, Linteris GT. Suppression of cup-burner flames using carbon dioxide in microgravity. Combust Flame 2004;137:506.
[35] Hirschfelder JC, Curtiss CF, Bird RB. Molecular theory of gases and liquids. New York: Wiley; 1954.
[36] Moran MJ, Shapiro HN. Fundamentals of engineering thermodynamics. 5th ed.; 2004.
[37] Szargut J, Morris DR, Stewart FR. Exergy analysis of thermal, chemical, and metallurgical processes. New York: Hemisphere; 1988.
[38] Katta VR, Goss LP, Roquemore WM. Numerical investigations of transitional H2/N2 jet diffusion flames. AIAA J 1994;32:84.
[39] Briones AM, Aggarwal SK, Katta VR. Effects of H_2 enrichment on the propagation characteristics of CH4-air triple flames. Combust Flame 2008;153:367–83.